Hindawi Publishing Corporation
Journal of Wind Energy
Volume 2014, Article ID 570234, 12 pages
http://dx.doi.org/10.1155/2014/570234

Research Article

Comparative Assessment of SVC and TCSC Controllers on the Small Signal Stability Margin of a Power System Incorporating Intermittent Wind Power Generation

T. R. Ayodele

Department of Electrical Engineering, Faculty of Technology, University of Ibadan, Ibadan 0037, Nigeria

Correspondence should be addressed to T. R. Ayodele; tayodele2001@yahoo.com

Received 9 August 2014; Accepted 24 November 2014; Published 11 December 2014

Academic Editor: Ujjwal K. Saha

Wind power is highly variable due to the stochastic behavior of wind speeds. This intermittent nature could excite the electromechanical modes resulting in the small signal instability of a power system. In this study, the performance of static VAR compensation (SVC) and thyristor controlled series capacitor (TCSC) controllers in the damping of electromechanical modes is analyzed and compared. The study employs probabilistic modal analysis method using Monte Carlo simulation and Latin hypercube sampling techniques. Various scenarios are created to get insight into the study. The results obtained from the modal analysis are verified by using the time-domain simulation. Some of the key results show that SVC is more robust in the damping of electromechanical modes compared to TCSC. The result also reveals that allocation of power system stabilizer (PSS) using probabilistic method is more effective and robust compared to deterministic approach.

1. Introduction

The complexity of power system has increased due to high rate of growth of power demands, and the increasing penetration of renewable energy generators (REGs) on the grid in recent years has further pushed the operation of the existing transmission lines closer to their operating limit. This has necessitated the need to understand the impact of REGs on the overall stability of a power system. The output power of most REGs (wind generators, PV, small hydrogenerators, etc.) is highly variable and can have considerable effect on the dynamic behavior of a power system leading to power swing and less synchronizing coupling [1]. Wind generators have been the most proliferated REG in recent time. This is a result of its technological maturity and the availability of wind resources in many regions of the world [2]. The present and the progressive scales of integration have generated concern about the possible impact it may have on the power system grid integrity. Most of the large wind farms are located where the wind resources are found; hence they are far from the load center and are connected to relatively weak grid [3]. The presence of wind generators connected to such weak transmission networks incurs serious concern about system stability, system security, and power quality. Small signal stability is a key issue in the study of grid impact of wind power integration as a result of its intermittent nature [4, 5]. Small signal stability is concerned with the ability of a power system to ascertain a stable operating condition following a small perturbation around its operating equilibrium [6]. Modal analysis is widely recognized for the analysis of small signal stability of a power system. The analysis is carried out based on the system nonlinear equations describing the dynamic behavior of the system, linearized about a chosen operating point.

In order to take into consideration the stochastic nature of wind power, probabilistic modal analysis method via Monte Carlo simulation (MCS) is employed using MATLAB based power system toolbox (PST). The wind speeds used for the generation of intermittent wind power are drawn from Weibull distribution using Latin hypercube sampling (LHS) techniques. The use of LHS reduces the number of iterations required in traditional MCS and hence reduces computational effort and cost. The basic outline of

the procedures for generating LHS as used in this paper is given in Appendix A. However, details on the application of LHS techniques to probabilistic small signal stability can be found in Ayodele et al.'s work [7].

FACTS controllers have been extensively used to improve the steady-state control problems and enhancing power system stability in addition to the main function of power flow control [8]. Damping electromechanical power oscillations has been recognized as an important issue in electric power system operation. Application of power system stabilizers (PSS), with increasing transmission line loading over long distances, may in many cases not provide sufficient damping for interarea power swings. In such cases, other solutions for power oscillation damping are needed. Fuzzy logic controlled energy storage (energy capacitor system) has been used to enhance the overall stability of electric power system [9]. Hossain et al. compared SVC and STATCOM in the improvement of voltage stability and concluded that STATCOM provides better response during low voltage compared to SVC [1]. The performance of three FACTS controllers, namely, static compensator (STATCOM), static synchronous series compensator (SSSC), and the unified power flow controller (UPFC), was studied in [10] using current injection model. The model was applied to damping electromechanical modes. According to their results, UPFC is the most effective FACTS controller for damping interarea oscillations and SSSC is more effective than STATCOM. Comparison of proportional integrated derivative (PID), power system stabilizer (PSS), and thyristor controlled dynamic brake (TCDB) in small signal stability study has been presented by Balwinder [11]. It was concluded that combination of PID with TCDB offers better improvement in oscillation damping. Application of controllable series compensator (CSC) in damping power system oscillation was investigated on the basis of Philip-Heffron model by Swift and Wang [12]. In their work, the capability of CSC controller was analyzed in terms of its damping torque contribution both for single machine infinite bus and for multimachine power system. The same authors later compared the effectiveness of damping torque of FACTS devices, namely, SVC, CSC, and phase shifter (PS), to power system [13]. It was concluded that SVC and CSC damping provide more damping torque during high load conditions while PS damping control does not depend on system load condition. However, none of the aforementioned study compared SVC and thyristor controlled series capacitor (TCSC) controllers. Moreover, none of the studies incorporates wind power in their study. In the present study, SVC and TCSC controllers are compared for the damping of electromechanical mode of a wind generator connected power system considering the intermittent nature of wind power using probabilistic approach.

2. Model Description

Analysis of small signal stability in an interconnected power system requires adequate model describing various components making up the system. Therefore, this section presents the model approach of these components.

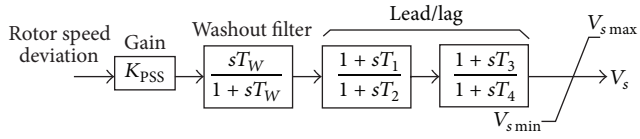

Figure 1: PSS block diagram design.

2.1. Synchronous Generator Model. Synchronous machine can be mathematically modeled as either elementary classical models or detailed ones. In the detailed models, transient and subtransient phenomena are considered [14, 15]. In this study, detailed model is employed to model all the synchronous generators.

The mechanical variables are linked with the electrical variables using the following [16]:

$$\begin{aligned} \left(D + T_j S\right) &= T_m - \left(E_q'' I_q + E_d'' I_d\right), \\ S\delta &= \omega - 1, \end{aligned} \tag{1}$$

where D and T_j represent the damping constant and the inertia time constant, respectively; T_m stands for the input mechanical torque; ω and δ represent the rotational speed and rotor angle, respectively; E_d'' and E_q'' correspond to the subtransient generated voltage in the direct and quadrature axes; and I_d and I_q stand for the armature current in the direct and quadrature axes, respectively.

2.2. Power System Stabilizer (PSS) Model. The input signal to PSS may be rotor speed, rotor angle, or a combination of this signal. The linearized differential equation of PSS can be written as follows [11]:

$$\frac{d\Delta X_{W(\text{Pss})}}{dt} = K_{\text{PSS}}\Delta\dot{\omega} - \frac{1}{T_W}\Delta X_{W(\text{PSS})}, \tag{2}$$

$$\frac{d\Delta X_{(\text{Pss})}}{dt} = \frac{T_1}{T_2}\Delta\dot{X}_{W(\text{PSS})} + \frac{1}{T_2}\Delta X_{W(\text{PSS})} - \frac{1}{T_2}\Delta X_{W(\text{PSS})}, \tag{3}$$

$$\frac{d\Delta V_{s(\text{Pss})}}{dt} = \frac{T_3}{T_4}\Delta\dot{X}_{(\text{PSS})} + \frac{1}{T_4}\Delta X_{(\text{PSS})} - \frac{1}{T_4}\Delta V_{s(\text{PSS})}, \tag{4}$$

where $d\Delta X_{W(\text{Pss})}$ represent the output of washout filter, $d\Delta X_{(\text{Pss})}$ represent the output of first lag-lead network, ΔV_s is the output signal of PSS block, and T_W is the washout time constant. T_1 and T_3 are lead-time constants while T_2 and T_4 are the lag time constants of lag-lead network. Figure 1 depicts the PSS block diagram design.

2.3. SVC Controller Model. Facts controllers are electronic devices that are used to enhance power system performance [17]. SVC is used to inject a controlled capacitance or inductive current in order to control specific variables, mainly bus voltage [18]. There are basically two configurations of SVC: the fixed capacitor (FC) with thyristor controlled reactor (TCR) and the thyristor switched capacitor (TSC) with TCR. The model of SVC as implemented in PST software is depicted in Figure 2.

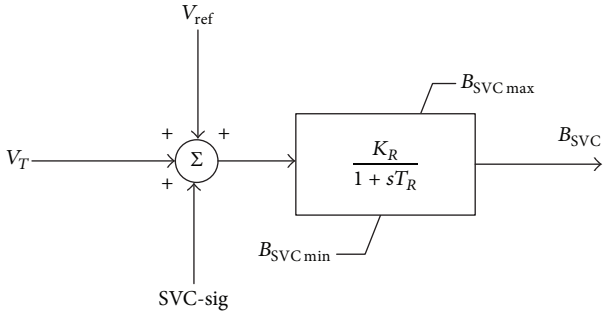

Figure 2: SVC model.

2.4. TCSC Controller Model. TCSC has proven to be very robust and effective in the of power system oscillations. The damping effect is obtained by inserting the TCSC in the interconnecting transmission line and executing reactance modulation in phase with the speed difference between the generators connected to the two terminals of the line. The damping effect of TCSC has the following benefits [19]. The effectiveness of the TCSC for controlling power swings increases with higher levels of power transfer, the damping effect of a TCSC on an inertia is unaffected by the location of the TCSC, the damping effect is insensitive to the load characteristic, when a TCSC is utilized to damp interarea modes, and it does not excite any local modes in the process [18]. The TCSC model as implemented in this paper is shown in Figure 3 where X_m is the stability control modulation reactance value which is determined by the stability or dynamic control loop, X_{eo} is the steady state reactance or set point of the TCSC whose value is determined by the steady state control loop, and X_e is the equivalent capacitive reactance of the TCSC.

2.5. Wind Energy Conversion System Model

2.5.1. Wind Speed Model. The intermittent nature of wind power is a result of the stochastic nature of wind speed which is the prime mover of any wind energy conversion system; therefore, adequate model of wind speed that will capture the variability of wind power is required. In this study, the wind speed is modelled using two-parameter Weibull distribution which is found to be appropriate for modelling wind speed in many regions of the world [20–22]. Two-parameter Weibull distribution can be represented as (5) [23] where $f_W(v)$ is the probability of observing wind speed (v) and k and c are the Weibull shape and scale parameters of the distribution, respectively. The shape and the scale parameters are provided in Table 7 in the Appendix B:

$$f_W(v) = \frac{k}{c}\left(\frac{v}{c}\right)^{k-1} \exp\left[-\left(\frac{v}{c}\right)^{k}\right]. \tag{5}$$

2.5.2. Wind Generator Model. The variable speed wind turbine is being considered as the most promising among the technologies for grid connection of wind generators today. However, a significant number of fixed speed wind turbines are still in operation. In this study, fixed speed wind generator made of squirrel cage induction generator (SCIG) is employed. Figure 4 gives the schematic diagram of the electrical power output (P_e) of a typical wind turbine. Not all the energy in the mass of moving air can be converted into electrical power. The amount of energy that can be converted into useful electrical power depends on the coefficient of the performance of the turbine, the transmission efficiency, and the generator efficiency. This can be written as

$$P_e = \frac{1}{2}\rho A C_p \eta_m \eta_g v^3, \tag{6}$$

where C_p is the coefficient of the performance of the turbine; it is a function of the tip speed ratio and the pitch angle. Theoretically, it has a maximum value of 0.59 known as the Betz limit. η_m is the mechanical transmission efficiency and η_g is the generator efficiency. The generated active power of wind generator was modeled as [22]

$$P_{e(v_i)} = \begin{cases} P_r \dfrac{v_i^2 - v_{\text{ci}}^2}{v_r^2 - v_{\text{ci}}^2}, & \left(v_{\text{ci}} \le v_i \le v_r\right), \\ P_r = \dfrac{1}{2}\rho A C_p \eta_m \eta_g v_r^3, & \left(v_r \le v_i \le v_{\text{co}}\right), \\ 0, & \left(v_i \le v_{\text{ci}},\ v_i \ge v_{\text{co}}\right), \end{cases} \tag{7}$$

where v_i is the vector of wind speeds generated according to the Weibull distribution of known parameters, $P_{e(v_i)}$ is the vector of active wind power generated in accordance with the stochastic wind speed and power curve of a wind turbine, v_{ci} is the cut-in wind speed, v_r is the rated wind speed, v_{co} is the cut-out wind speed, and P_r is the rated power. The parameters of the wind turbine are provided in Table 7 in Appendix B.

2.5.3. Reactive Power Model of Wind Generator. The active power injected into the grid is derived from the power curve of the wind turbine with the prior knowledge of wind speed and its distribution. The reactive power absorbed or injected from or into the grid, respectively, can be derived using the steady state equivalent circuit of an asynchronous induction generator as shown in Figure 5, where U is the terminal voltage, X_1 is the stator reactance, X_2 is the rotor reactance, X_m is the magnetising reactance, and r_2 is the rotor resistance. The stator resistance is neglected. From the circuit, the real power injected to the grid can be calculated as

$$P_{e(v_i)} = \frac{-U^2\left(r_2/s_i\right)}{\left(r_2/s_i\right)^2 + X^2}, \tag{8}$$

where $X = X_1 + X_2$ and $P_{e(v_i)}$ is the generated active power at different wind speeds according to the power curve in (3). The amount of reactive power absorbed from the grid depends on the rotor slip s_i, which also changes as the wind power varies in accordance with the variations in wind speed. Based on (8), s_i was derived as (9). The reactive power $Q_{(v_i)}$ absorbed at

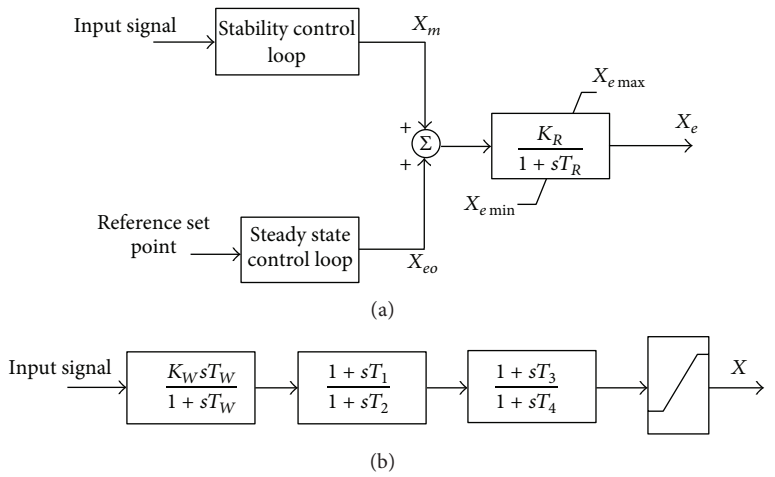

Figure 3: (a) TCSC model for stability study and (b) TCSC stability control loop.

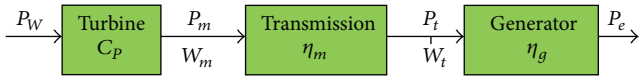

Figure 4: Block diagram of wind generator electrical power output.

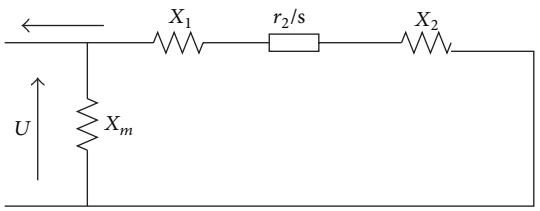

Figure 5: State equivalent circuit of an asynchronous generator.

different wind speeds can be computed as (10). Consider the following:

$$s_i = \frac{-Ur_2 + \sqrt{U^4 r_2^2 - P_{e(v_i)}^2 X^2 r_2^2}}{2P_{e(v_i)}X^2} \tag{9}$$

$$Q_{(v_i)} = \frac{s_i^2 X\left(X + X_m\right) + r_2^2}{s_i X_m r_2} P_{e(v_i)}. \tag{10}$$

Different slip and reactive power can be obtained from the relation between active power and reactive power for different generated active power, depending on the wind speed.

2.5.4. Wind Farm Model. The combination of several WECS constitutes a wind farm which may be of the same type or different types. The power output of a wind farm is the total sum of the output power of individual WECS. For a wind farm with N numbers of WECS, the output power of the wind farm ($P_{e(v_i)wf}$) at different wind speeds (v_i) can be written as

$$P_{e(v_i)wf} = \sum_{k=1}^{N} n_k P_{e(v_i)k}, \tag{11}$$

where n_k indicates the number of WECS of type k and $P_{e(v_i)k}$ is the output electrical power of type k WECS. Similarly, the reactive power absorbed by the wind farm can be expressed as

$$Q_{(v_i)wf} = \sum_{k=1}^{N} n_k Q_{(v_i)k}. \tag{12}$$

For a wind farm consisting of the same types of wind turbines, (11) and (12) become (13) and (14). Consider the following:

$$P_{e(v_i)wf} = NP_{e(v_i)}, \tag{13}$$

$$Q_{(v_i)wf} = NQ_{(v_i)}. \tag{14}$$

3. Power System and Small Signal Stability Model

The dynamic model of power system with wind turbines can be modeled as a set of nonlinear differential algebraic equation:

$$\dot{x} = f\left(x, y, p\right), \tag{15}$$

$$0 = g\left(x, y, p\right), \tag{16}$$

where x is the dynamic state variable which is directly defined by (15) and y is the instantaneous variable such that the system satisfies the constraint in (16). The parameter p defines a specific system configuration and the operating condition. The state matrix can be obtained by linearizing the system power flow equations.

Choosing the equilibrium point (x_o, y_o, p_o), (15) and (16) are linearized by taking the first order Taylor expansion as (17) and (18), respectively. Consider the following:

$$\Delta\dot{x} = F_x \Delta x + F_y \Delta y, \tag{17}$$

$$0 = G_x \Delta x + G_y \Delta y. \tag{18}$$

If G_y is nonsingular matrix, then

$$\Delta\dot{x} = \left(F_x - F_y G_y^{-1} G_x\right)\Delta x,$$
$$A = F_x - F_y G_y^{-1} G_x, \tag{19}$$

where F_x, F_y, G_x, and G_y are power flow Jacobian matrices. Hence the small signal stability analysis for the model can be obtained as

$$\Delta\dot{x} = A\Delta x. \tag{20}$$

The value of λ that satisfies (21) is the eigenvalues of matrix A. It contains information about the response of the system to a small perturbation:

$$\det(\lambda I - A) = 0. \tag{21}$$

The eigenvalue can be real and/or complex. The complex values appear in conjugate pairs if A is real (22). The complex eigenvalues are referred to as oscillatory modes and they appear in conjugate:

$$\lambda_i = \sigma_i \pm j\omega_i. \tag{22}$$

Each eigenvalue represents a system mode and the relationship between this mode and the stability is given by Lyapunov's first method [14].

The frequency of oscillation in, Hz, and the damping ratio are given by

$$f = \frac{\omega_i}{2\pi},$$
$$\xi = \frac{-\sigma_i}{\sqrt{\sigma_i^2 + \omega_i^2}}. \tag{23}$$

The contributions of states on oscillation can be observed by evaluating the participation factors (PFs) of each state on a particular mode. Participation factor gives the relationship among the states and eigenmode in a dynamic system [14]. The participation factor of mode i, can be computed using [24]

$$p_i = \begin{pmatrix} p_{1i} \\ p_{2i} \\ \vdots \\ p_{mi} \end{pmatrix},$$
$$p_{ki} = \frac{|\Phi_{ki}||\Psi_{ik}|}{\sum_{k=1}^{n} |\Phi_{ki}||\Psi_{ik}|}, \tag{24}$$

where m is the number of state variables, p_{ki} is the participation factor of the kth state variable into mode i, Φ_{ki} is the ith element of the kth right eigenvector of A, and Ψ_{ik} is the mth element of the ith left eigenvector of A.

4. System under Study

An IEEE 4-machine, 2-area network as depicted in Figure 6 is used for the study.

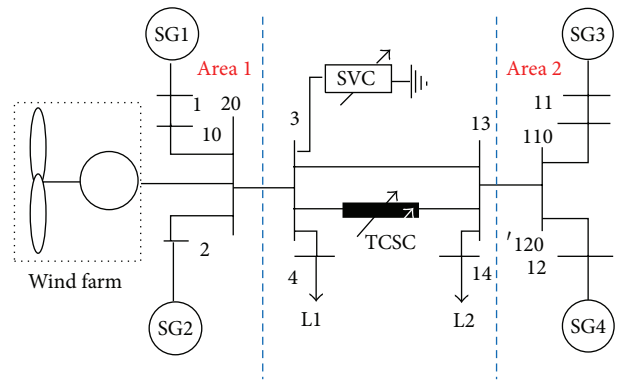

Figure 6: Modified IEEE 4-machine, 2-area network consisting of wind generators.

The network is selected because it consists of two areas interconnected by weak tie-line which makes it suitable for studying interarea modes. Moreover, the network parameters are readily available and this will enhance repeatability of the work. The network is slightly modified to incorporate wind farm at bus 20. The wind farm consists of 50 different wind generators made of SCIG technology and each is of 2 MW. The network also consists of four conventional synchronous generators at buses 1, 2, 11, and 12. SVC is connected to bus 3 while TCSC is connected on the line connecting buses 3 and 13. The data used for the load flow can be found in [25]; the data not found in the reference due to modification to the network are provided in Appendix B.

The flow chart of Monte Carlo simulation algorithm for the analysis of small signal stability is depicted in Figure 7 and is programmed based on power system toolbox (PST) [25] in MATLAB.

The analysis begins with the generation of wind speed for the wind turbine using Weibull distribution through LHS method. An earlier study showed that, for small signal stability application, 100 runs of input variables generated using LHS are appropriate in Monte Carlo simulation to achieve reasonable results [7]. The load flow analysis is carried out next using Newton-Raphson algorithm, followed by the damping ratio computation via modal analysis. Finally, the results are analysed statistically.

5. Scenario Creation, Results, and Discussion

Four scenarios (Case A–Case D) are created in order to gain meaningful insight into the study. The description and the results of each scenario are discussed under each case.

5.1. Case A: Original Network (No Wind Farm Connected and No Controllers Connected). The base case is made up of the original network without considering the wind farm and the controllers (PSS, SVC, and TSCS). This is to know the initial state of the network in terms of small signal stability and hence the impact of the controllers when they are later added. The result of the simulation shows that there are total of 55 modes in which 24 are oscillatory which appears in

Table 1: Oscillatory modes before wind power integration.

Number	Modes $\lambda_i = \sigma_i \pm j\omega_i$	Damping ratio (ξ)	Frequency (f)
5 and 6	-0.236 ± 0.520	0.413	0.083
7 and 8	-0.238 ± 0.525	0.414	0.084
9 and 10	-0.249 ± 0.645	0.360	0.103
11 and 12	-0.492 ± 0.986	0.446	0.157
13 and 14	-0.800 ± 1.322	0.518	0.210
21 and 22	-0.009 ± 3.586	0.0024	0.571
25 and 26	-0.4780 ± 6.885	0.069	1.096
27 and 28	-0.488 ± 6.932	0.070	1.103
33 and 34	-8.587 ± 9.555	0.668	1.521
35 and 36	-8.605 ± 9.792	0.660	1.558
37 and 38	-8.718 ± 10.064	0.655	1.612
39 and 40	-8.722 ± 10.071	0.655	1.603

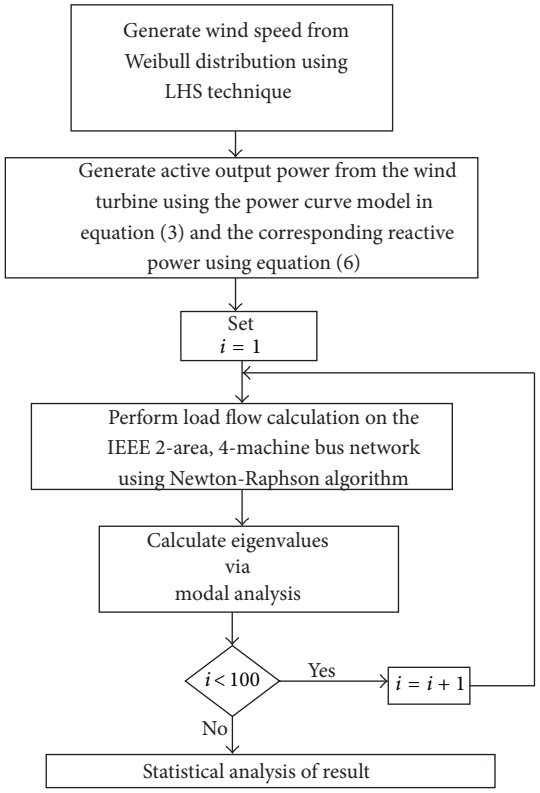

Figure 7: The flowchart of MCS based small signal stability.

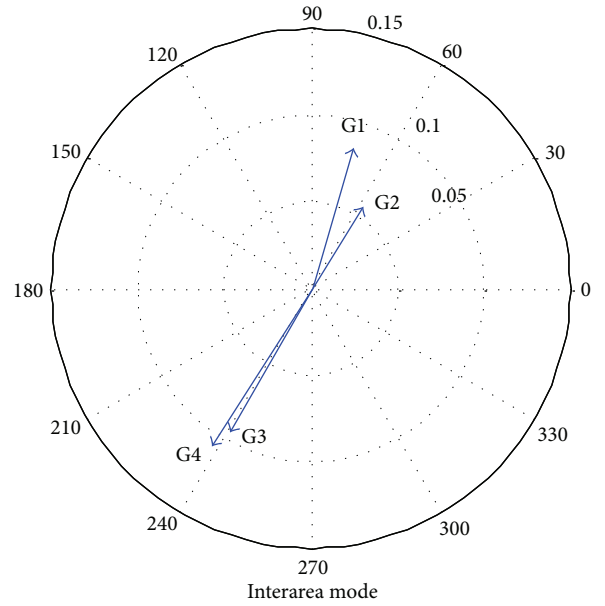

Figure 8: Compass plot of interarea mode.

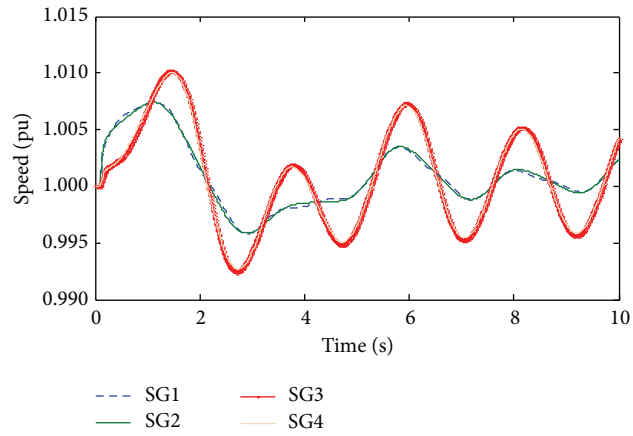

Figure 9: Speed deviation when 3-phase fault of duration 100 ms was created at the middle of the line connecting buses 3 and 101.

12 conjugate pairs. The results of the oscillatory mode are depicted in Table 1. In small signal stability studies, the modes of interest are the electromechanical modes. These modes must be properly damped for a small signal secured power system. Three conjugate pairs of electromechanical modes are identified and are shown in Table 2. The table depicts that there is one conjugate pair of interarea modes (modes 21 and 22) with damping ratio of 0.24% and oscillatory frequency of 0.571. Figure 8 depicts the compass plot confirming that modes 21 and 22 are interarea modes with generators in area 1 (SG1 and SG2) oscillating against generators in area 2 (SG3 and SG4). Two conjugate pairs are identified as local modes (modes 9 and 10 and modes 27 and 28) with damping ratio of 36% and 7%, respectively. All the modes are positively and strongly damped with damping ratio greater than 5% except the interarea mode which has a damping ratio of 0.24%. The interarea mode determines the stability of the system; it can therefore be concluded that the original network is weakly damped. The results were confirmed using time domain simulation. A 3-phase fault of duration 100 ms was created at the middle of lines connecting buses 3 and 13; the result is depicted in Figure 9. It can be observed from the figure that the oscillation in the speed of the generators neither dies out nor grows signifying a weakly damped system. This confirms the result of the modal analysis. The figure also reveals the interarea oscillation between the generators in area 1 and the generators in area 2.

Table 2: Electromechanical modes for Case A (base case, i.e., no wind farm connected and no controllers).

Number	Mode $\lambda_i = \sigma_i \pm j\omega_i$	Type	Damping ratio (ξ)	Frequency (f)	Participation (p_i)
9 and 10	−0.249 ± 0.645	Area 1 local	0.360	1.523	SG3 and SG4
21 and 22	**−0.009 ± 3.586**	**Interarea**	**0.0024**	**0.571**	**SG1, SG2, SG3, and SG4**
27 and 28	−0.488 ± 6.932	Area 2 local	0.070	1.103	SG1 and SG2

Table 3: Electromechanical mode for Case B (wind farm connected to bus 20 and no controllers).

Number	Type of mode	Mean mode $\lambda_i = \sigma_i \pm j\omega_i$	Damping ratio (ξ)		Frequency (f)	
			Mean	SD	Mean	SD
9 and 10	Area 1 local	$-0.547 \pm 7.381i$	0.065	0.007	1.177	0.0015
21 and 22	**Interarea**	**0.061 ± 4.018i**	**−0.015**	**0.0029**	**0.639**	$\mathbf{4.9 * 10^4}$
27 and 28	Area 2 local	$-0534 \pm 7.314i$	0.076	$2.84 * 10^4$	1.164	0.0016

5.2. Case B (Wind Farm Is Connected at Bus 20 to the Network in Case A). Wind farm made of 50 wind power generators each of 2 MW was connected to bus 20. Again no controller was considered. This will allow us to know the impact of the wind power on the small signal stability of the original network. The wind power was generated as described in the flowchart in Figure 7. The result was statistically analysed and presented in Table 3. From the table, it can be observed that the interarea mode is negatively damped with mean damping ratio of −0.015 signifying an unstable system. The standard deviation (SD) of the damping ratio is low (0.0029). This shows that, in all the operating condition (varying wind power), the damping ratio is negative. Figure 10(a) shows that the interarea mode was weakly damped (with damping ration of 0.0024) before wind farm was connected. However, the weakly damped interarea mode became unstable (shifted to the left side of the plane) when wind farm was connected to the network as shown in Figure 10(b). To verify this result, time domain simulation was carried out by creating a 3-phase fault of duration 100 ms at the middle of line connecting bus 3 to bus 13. The results showing both the electrical power and the speed of the four synchronous generators when wind farm was connected are presented in Figure 11. The figure confirms that the system is unstable when wind power was injected into the network. This is due to the interarea mode that is negatively damped after the wind farm was connected. The instability resulting from this mode can be vividly observed in Figure 11(b) with the generators in area 1 (SG1 and SG2) swinging against generators in area 2 (SG3 and SG4).

5.3. Case C (Power System Stabilizer Is Allocated to the Generators). The main function of power system stabilizer is to provide the synchronizing torque [14] and hence improve the damping of a power system. However, it has to be properly allocated to the most suitable synchronous generator in order to provide the most effective result. The aim here is to improve the damping of the interarea mode in Case B by allocating PSS. The allocation of PSS has been traditionally done using deterministic method in which a single operating condition is considered. In this paper, probabilistic approach is used in determining the most suitable synchronous generator to allocate the PSS in order to damp the interarea mode.

Table 4: Damping of interarea mode (modes 21 and 22).

Methods	Allocation	Damping ratio (ξ)
Deterministic	SG3	0.0076
Probabilistic	SG1	0.0726

The result is then compared with the deterministic method. Figure 12(a) shows the speed participation factor (PF) when deterministic method is used (i.e., single operating condition of wind speed is considered) while Figure 12(b) depicts the mean speed PF using probabilistic approach (i.e., all the operating conditions of wind speed are taken into consideration and the statistical average is determined). The result of the deterministic method as depicted in Figure 12(a) reveals that SG3 will be the generator that will provide the most effective damping when PSS is allocated while Figure 12(b) shows that SG1 should be installed with PSS for effective damping of the interarea mode.

PSS were allocated using the two methods and the results are presented in Table 4. The table shows that when PSS is allocated deterministically, the interarea mode in Case B improved from being negatively damped (−0.015) to being weakly damped (0.0076). However, when allocated probabilistically, the negatively damped interarea mode became strongly damped (0.0726). The result is again verified using time domain simulation and is presented in Figure 13. The figure confirms that probabilistic method presents a better allocation of PSS for small signal stability application.

5.4. Case D (SVC and TCSC Are Installed in Turns). SVC only was first installed on bus 3 in the network of Case B. This is to give insight into the influence of SVC on the small signal stability of a power system. The objective is to see its influence on the small signal stability and then compare its performance with that of TCSC. Thereafter, SVC was taken out and then TCSC only was installed on the line connecting bus 3 to bus 13. Both SVC and PSS were later installed to give insight into the combinational effect of the duo. Finally, SVC and PSS were taken out and both TCSC and PSS were installed. The results are presented in Table 5. The table shows that SVC has a better performance in the

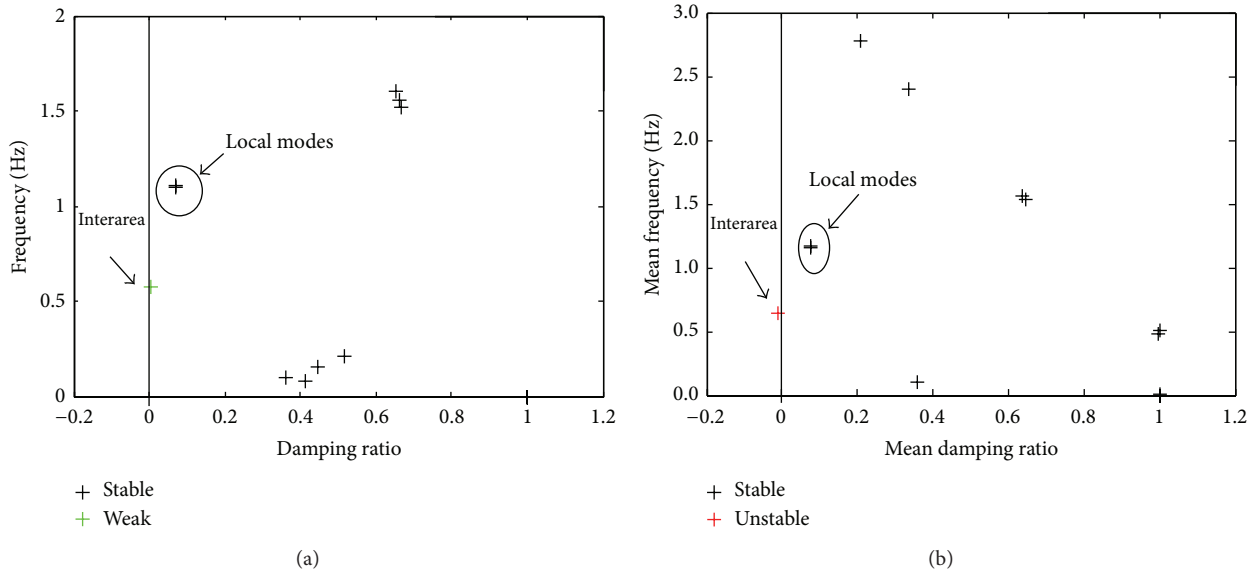

Figure 10: The plot of frequency versus damping ratio of the network: (a) without wind farm connected and (b) with wind farm connected.

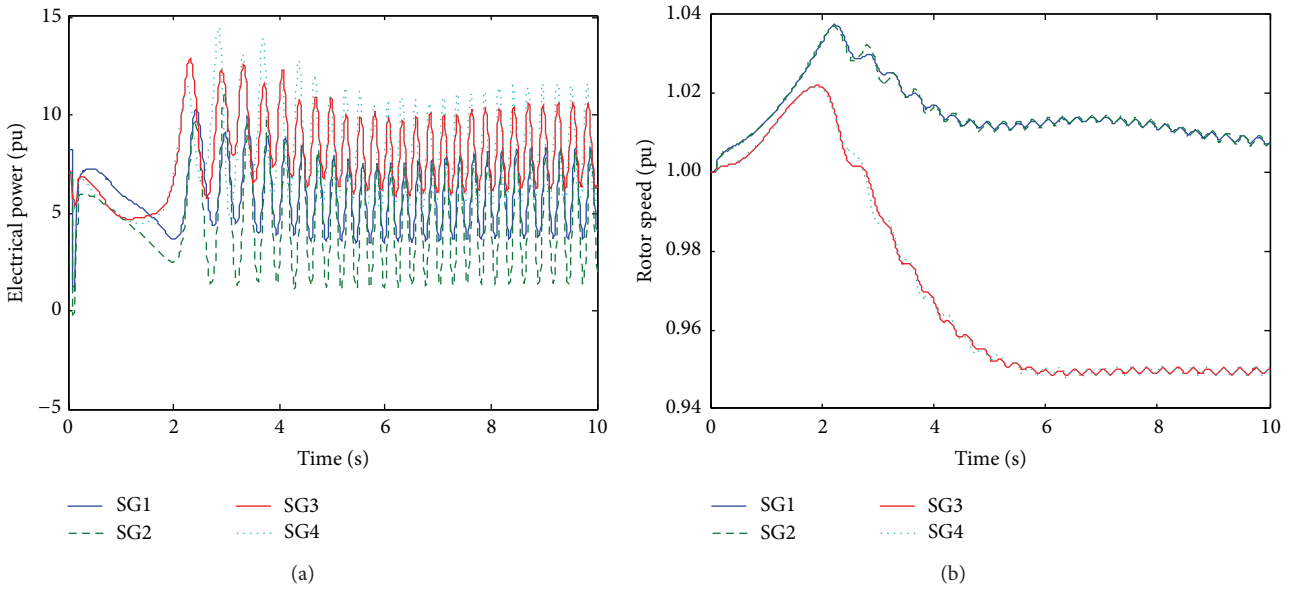

Figure 11: Time domain simulation showing (a) the electrical power and (b) the speed deviation when wind power was connected to the network.

damping of the interarea mode with mean damping ratio of 1.67% compared to that of TCSC with damping ratio of 0.61%. The combination of SVC and PSS provides effective damping compared to TCSC and PSS. The controllers are compared in Figure 14 for the damping of the interarea mode.

It can be viewed from the figure that the combination of SVC and PSS gives the best damping to the interarea mode with damping ratio of 15.54%. The order of performance of the controllers as used in this paper is as shown in Table 6. From the table, it can be seen that combination of SVC and PSS puts up the overall best performance followed by the combination of TCSC and PSS. It is generally observed that better results are obtained when the controllers are combined with PSS compared to when they are operated in a stand-alone mode.

Table 5: Influence of controllers in the damping of the interarea mode (modes 21 and 22).

	Damping ratio (ξ)		Frequency (f)	
	Mean	Std.	Mean	Std.
SVC only	0.0167	0.0011	0.6082	0.0038
TCSC only	0.0061	0.00069	0.6343	0.0010
SVC + PSS	0.1554	0.0021	0.6288	0.00098
TCSC + PSS	0.1032	0.0030	0.6270	0.0015

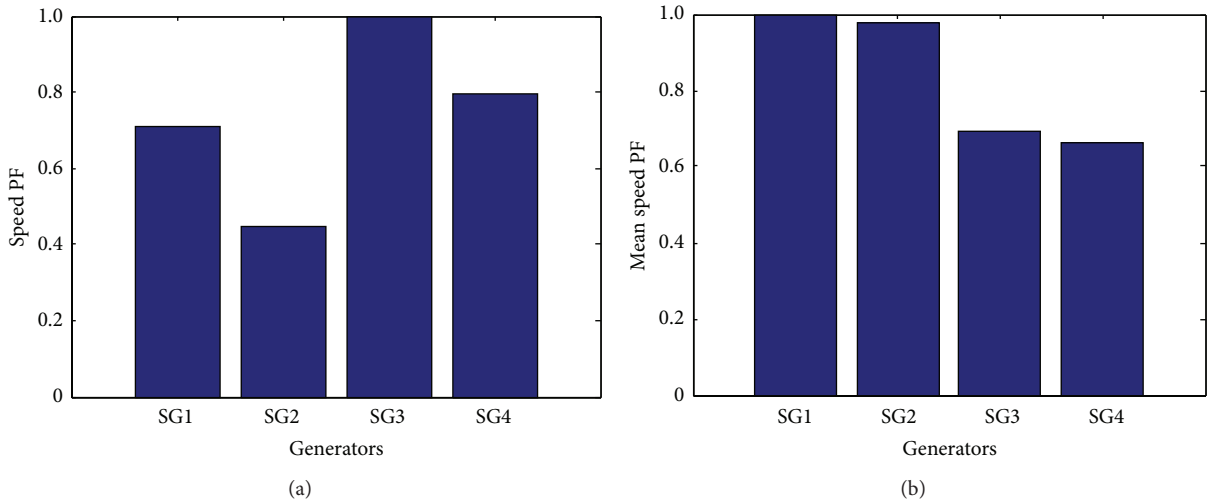

Figure 12: The bar plot of (a) speed participation factor using deterministic method and (b) mean speed participation factor using probabilistic method.

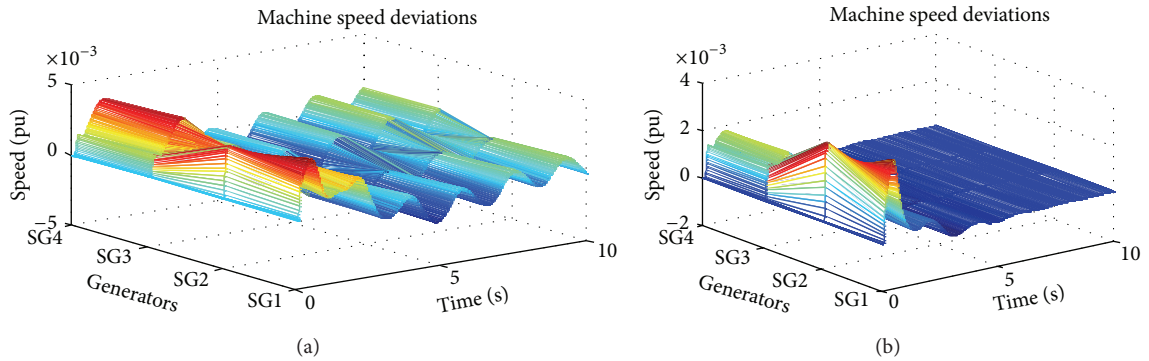

Figure 13: 3D plot of speed when PSS is allocated using (a) deterministic method and (b) probabilistic method.

Table 6: Order of performance of the controller(s) at damping electromechanical modes.

S/N	Controllers and possible combination	Order of performance
1	SVC + PSS	1st
2	TCSC + PSS	2nd
3	Probabilistic allocation of PSS only	3rd
4	SCV only	4th
5	Deterministic allocation of PSS only	5th
6	TCSC only	6th

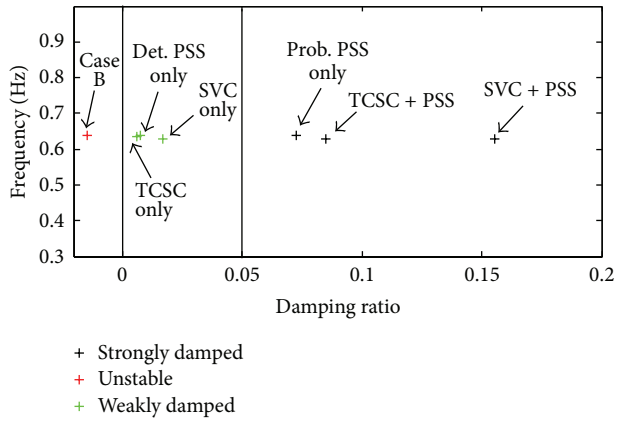

Figure 14: Comparison of performance of the controllers in the damping of the interarea mode.

The result of the modal analysis was confirmed with time domain simulation and the result is presented in Figure 15.

6. Conclusion

Comparative assessment of SVC and TCSC controllers and their combination with PSS at improving the electromechanical modes excited by the intermittent wind power generated from wind farm made of fixed speed squirrel cage induction generators has been studied using probabilistic modal analysis. Correctness of every result obtained by the modal analysis was verified using time domain simulation. It was revealed that combination of SVC and PSS performs best at damping the electromechanical modes followed by TCSC and PSS. It can be deduced that better performance of the controllers is obtained when combined with PSS compared to

Table 7: Turbine parameters.

Cut-in wind speed (v_{ci})	3.5 m/s	Rated turbine power (Pr)	2 MW
Rated wind speed (v_r)	10 m/s	Weibull shape parameter (k)	1.8
Cut-out wind speed (v_{co})	25 m/s	Weibull scale parameter (c)	10 m/s

Table 8: Induction generator parameters.

Stator resistance (r_1)	Neglected	Magnetizing reactance	3 pu
Rotor resistance (r_2)	0.009 pu	Inertial constant	4 s
Stator reactance (x_1)	0.01 pu	Mechanical transmission efficiency (η_m)	95%
Rotor reactance	0.009 pu	Generator efficiency (η_g)	95%

Table 9: Power system stabilizer parameters.

Parameters	Values	Parameters	Values
Lead time constant (T_1)	0.05	Washout time constant (T_W)	10
Lag time constant (T_2)	0.015	Maximum output limit ($\Delta V_{s(\max)}$)	0.2
Lead time constant (T_3)	0.08	Minimum output limit ($\Delta V_{s(\min)}$)	−0.05
Lag time constant (T_4)	0.01	PSS gain (K_{PSS})	100 pu

when operating as a stand-alone controller. It has also been shown that allocation of PSS using probabilistic techniques enhances damping of electromechanical mode compared to the deterministic allocation. This is because, in probabilistic allocation, various combinations of wind power scenarios are taken into consideration unlike deterministic method that takes into consideration only single scenario. The future study will focus on the use of variable speed generator using DFIG and optimal location of SVC for effective damping of interarea mode excited by intermittent wind power. In this study, conclusions are made based on 4-machine, 2-area network; further work will consider large network that will give room for more scenario consideration.

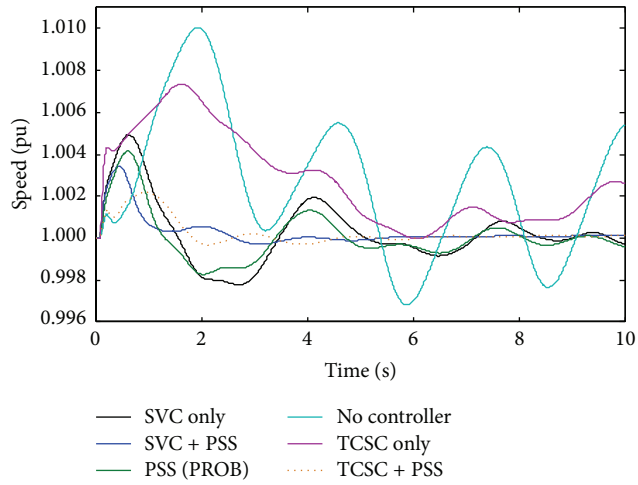

Figure 15: Time domain simulation comparison of the controllers for damping interarea modes.

Appendices

A. Latin Hypercube Sampling Techniques

The basic sampling procedures as applied to probabilistic small signal stability in this paper are as follows.

(i) Let $G_1, \ldots, G_N$ be the N input random variables in a probability problem. The cumulative distribution of G_n which belongs to $G_1, \ldots, G_N$ can be written as

$$Y_n = F_n(G_n). \tag{A.1}$$

For a sample size k, the range of Y_n from $[0, 1]$ is divided into k nonoverlapping intervals of equivalent length; hence the length of each interval is given as $1/k$.

(ii) One sample value is chosen from each interval randomly without replacement. Then, the sampling values of G_n can be calculated by the inverse function. The nth sample of G_n can be determined by

$$G_{nk} = F_n^{-1}\left(\frac{n - 0.5}{k}\right). \tag{A.2}$$

(iii) The sample value of G_n can now be assembled in a row of the sampling matrix as given in

$$[G_{n1}, G_{n2}, \ldots, G_{nk} \ldots, GnN]. \tag{A.3}$$

Once all the k input random variables are sampled, an $N \times K$ primary sampling G can be obtained. LHS can always start with the generation of uniform distributed samples in interval $[0, 1]$ then inverting the cumulative distribution function (CDF) to obtain the target distribution.

B. Parameters Used in the Study

See Tables 7, 8, 9, 10, and 11.

Table 10: SVC parameters.

Parameters	Values	Parameters	Values
Maximum susceptance ($B_{\text{svc max}}$)	1 pu	Regulator gain (K_R)	10
Minimum susceptance ($B_{\text{svc min}}$)	−1 pu	Regulator time constant (T_R)	0.05 s

Table 11: TCSC controller parameters.

T (s)	K_W (pu)	T_W (s)	T_1 (s)	T_2 (s)	T_3 (s)	T_4 (s)	$X_{\min}$ (pu)	$X_{\max}$ (pu)
0.015	1.1	5	1.1	0.05	0.08	0.5	0.00527	0.0514

Conflict of Interests

The author declares that there is no conflict of interests regarding the publication of this paper.

References

[1] M. J. Hossain, H. R. Pota, M. A. Mahmud, and R. A. Ramos, "Impacts of large-scale wind generators penetration on the voltage stability of power systems," in *Proceedings of the IEEE Power and Energy Society General Meeting*, pp. 1–8, San Diego, Calif, USA, July 2011.

[2] T. R. Ayodele, A. A. Jimoh, J. L. Munda, and J. T. Agee, "Challenges of grid integration of wind power on power system grid integrity: a review," *International Journal of Renewable Energy Research*, vol. 2, no. 4, pp. 618–626, 2012.

[3] M. R. Rathi and N. Mohan, "A novel robust low voltage and fault ride through for wind turbine application operating in weak grids," in *Proceedings of the 31st Annual Conference of IEEE Industrial Electronics Society (IECON '05)*, pp. 2481–2486, November 2005.

[4] Â. Mendonça and J. A. Peças Lopes, "Impact of large scale wind power integration on small signal stability," in *Proceedings of the International Conference on Future Power Systems*, Amsterdam, The Netherlands, November 2005.

[5] L. B. Shi, C. Wang, L. Z. Yao, L. M. Wang, and Y. X. Ni, "Analysis of impact of grid-connected wind power on small signal stability," *Wind Energy*, vol. 14, no. 4, pp. 517–537, 2011.

[6] X. Li, Z. Zeng, J. Zhou, and Y. Zhang, "Small signal stability analysis of large scale variable analysis of large scale variable speed wind turbines integration," in *Proceedings of the International Conference on Electrical Machines and Systems (ICEMS '08)*, pp. 2526–2530, Wuhan, China, 2008.

[7] T. R. Ayodele, A. A. Jimoh, J. L. Munda, and J. T. Agee, "Performance evaluation of sampling techniques in Monte Carlo simulation–based probabilistic small signal stability analysis," in *Proceedings of the 23rd IASTED International Conference on Modelling and Simulation (MS '12)*, Banff, Canada, 2012.

[8] W. Qiao, R. G. Harley, and G. K. Venayagamoorthy, "Effects of FACTS devices on a power system which includes a large wind farm," in *Proceedings of the IEEE PES Power Systems Conference and Exposition (PSCE '06)*, pp. 2070–2076, IEEE, Atlanta, Ga, USA, November 2006.

[9] S. Ibrahim, "Eigenvalue based stability improvement of electric power systems through voltage regulation," *International Journal of Renewable Energy Research*, vol. 3, no. 2, pp. 383–387, 2013.

[10] p. Jungsoo, J. Gilsoo, and M. S. Kwang, "Modeling and control of VSI type FACTS controllers for power system dynamic stability using the current injection method," *International Journal of Control, Automation and Systems*, vol. 6, no. 4, pp. 495–505, 2008.

[11] S. S. Balwinder, "Linearized modeling of single machine infinite bus power system and controllers for small signal stability investigation and enhancement," *International Journal of Advanced Research in Computer Engineering & Technology*, vol. 1, no. 8, pp. 21–28, 2012.

[12] F. J. Swift and H. F. Wang, "Application of the controllable series compensator in damping power system oscillations," *IEEE Proceeding—Generation, Tranmision, Distribution*, vol. 143, no. 4, pp. 359–364, 1996.

[13] H. F. Wang and F. J. Swift, "A unified model for the analysis of facts devices in damping power system oscillations part I: single-machine infinite-bus power systems," *IEEE Transactions on Power Delivery*, vol. 12, no. 2, pp. 941–946, 1997.

[14] P. Kundur, *Power System Stability and Control*, vol. 1 of *The EPRI Power System Engineering*, McGraw-Hill, New York, NY, USA, 1994.

[15] J. Arrillaga and C. P. Arnoid, Eds., *Computer Analysis of Power Systems*, John Wiley and Sons, Chichester, UK, 1990.

[16] P. M. Anderson and A. A. Fouad, Eds., *Power System Control and Stability*, IOWA State University Press, Ames, Iowa, USA, 1977.

[17] N. Mithulananthan, M. M. A. Salama, C. A. Cañizares, and J. Reeve, "Distribution system voltage regulation and var compensation for different static load models," *International Journal of Electrical Engineering Education*, vol. 37, no. 4, pp. 384–395, 2000.

[18] S. K. M. Kodsi and C. A. Canizares, "Modelling and simulation of IEEE 14 bus system with fact controllers," Technical Report 2003-3, 2003.

[19] R. Grünbaum, A. Sannino, and C. Wahlberg, *Use of FACTS for Eenhanced Flexibility and Efficiency in Power Transmission and Distribution Grids*, 2012.

[20] T. R. Ayodele, A. A. Jimoh, J. L. Munda, and J. T. Agee, "The influence of wind power on the small signal stability of a power sysyem," in *Proceedings of the International Conference on Renewable Energy and Power Quality (ICREPQ '11)*, Las Palmas de Gran Canaria, Spain, 2011.

[21] T. R. Ayodele, A. A. Jimoh, J. L. Munda, and J. T. Agee, "A statistical analysis of wind distribution and wind power potential in the coastal region of South Africa," *International Journal of Green Energy*, vol. 10, no. 8, pp. 814–834, 2013.

[22] T. R. Ayodele, A. A. Jimoh, J. L. Munda, and J. T. Agee, "Impacts of tie-lines and wind generator location on small signal stability of a power system," *International Journal of Renewable Energy Research*, vol. 3, no. 1, pp. 51–59, 2013.

[23] M. Veigas and G. Iglesias, "Evaluation of the wind resource and power performance of a turbine in Tenerife," *Journal of*

Renewable and Sustainable Energy, vol. 4, no. 5, Article ID 053106, 2012.

[24] F. Mei and B. C. Pal, "Modelling and small-signal analysis of a grid connected doubly-fed induction generator," in *Proceedings of the IEEE Power Engineering Society General Meeting*, pp. 2101–2108, San Francisco, Calif, USA, June 2005.

[25] J. Chow, *Power System Toolbox 2.0—Dynamic Tutoria and Functions*, Cherry Tree Scientific Software, 2000.